We are IntechOpen, the world's leading publisher of Open Access books Built by scientists, for scientists

4,800
Open access books available

122,000
International authors and editors

135M
Downloads

Our authors are among the

154
Countries delivered to

TOP 1%
most cited scientists

12.2%
Contributors from top 500 universities

WEB OF SCIENCE™

Selection of our books indexed in the Book Citation Index in Web of Science™ Core Collection (BKCI)

Interested in publishing with us?
Contact book.department@intechopen.com

Numbers displayed above are based on latest data collected.
For more information visit www.intechopen.com

8

Determination of Aspect-Ratio Distribution in Gold Nanowires Using Absorption Spectra and Transmission Electron Microscopy Techniques

Hiroo Omi
NTT Basic Research Laboratories, NTT Corporation, Japan

1. Introduction

The surface plasmon excitation energies of noble metal nanowires are strongly dependent on the dimensions of the nanowire and the local environment, which allows for tunable optical characteristics of nanowire samples (Noguez, 2007; Nehl, C. L. & Hafner, J. H. 2008). This has great advantages for the use of nanowires in surface-enhanced Raman spectroscopy (Orendorff et al. 2006; Sztainbuch, 2006; Suzuki et al. 2004, 2005), medical imaging, disease treatment, and other applications such as highly sensitive sensors (Agarwal et al. 2007; Gibbons et al. 2006; Yu & Irudayaraj 2007; Chen et al. 2007). For this reason, the fabrication processes for nanowires and the characterization of their optical properties are of great interest in current research (Murphy et al. 2006; Gulati et al. 2006; Miranda & Ahmadi 2005; Zweifel & Wei 2005; Hu et al. 2003; Sönnichsen et al. 2002). It would be useful to have a quick and easy way to accurately determine the size distribution of nanoparticles in solution in order to analyze nanowire synthesis processes or characterize samples for applications.

In 1912, Gans extended Mie's theory of the scattering of spherical particles (Mie 1908) for the case of oblate and prolate spheroids (Gans 1912). This simple theory describes the absorption characteristics of spheroidal particles smaller than the excitation wavelength and could provide a reasonable approximation for the optical characteristics of nanowires with different geometries. Because absorption measurements are simple, fast, and can be done in situ during the growth process, they would offer an excellent basis for particle characterization.

Nanowire synthesis always leads to dispersion in the nanowire aspect ratios, commonly defined as the length of the particle divided by its width. It has been well established that the absorption spectrum of a particle is strongly dependent on this aspect ratio (Gulati et al. 2006; Link et al. 2005; Yan et al. 2003; Link & El-Sayed 2005; Prescott & Mulvaney 2006; Brioude et al. 2005; Murphy et al. 2005; Pérez-Juste et al. 2005). The absorption spectrum of a disperse nanowire solution will therefore be broadened, and information on the

aspect-ratio distribution is thus contained in a measured absorption spectrum (Eustis et al. 2006).

Comparisons of experimentally determined absorption spectra and numerical approximations with Gans theory (Prescott & Mulvaney 2006; Brioude et al. 2005) suggest that there is a non-negligible dependence of the absorption spectrum on the end-cap geometry and particle size. Prescott and Mulvaney (Prescott & Mulvaney 2006) used discrete dipole approximation (DDA) calculations to determine the importance of the exact gold nanowire shape. They noticed an improvement over Gans theory by modeling the rods as cylinders. Gans theory uses perfect spheroids instead. However, they observed the presence of spherical end caps and admitted that the actual particle geometry is not described correctly by a cylinder. On the basis of their DDA model, they suggested shape factors that take into account the particle width, end-cap geometry, and aspect ratio. These shape factors are empirically derived, and there is no explanation for why the proper particle geometry (a cylinder with oblate spheroids as end caps) does not give an accurate absorption spectrum. We are therefore led to the hypothesis that there must be an additional physical quantity that is variable.

Previous papers (Yan et al. 2003; Link & El-Sayed 2005; Prescott & Mulvaney 2006; Brioude et al. 2005) have systematically reported calculated longitudinal plasmon excitation peak positions that are too low compared to various experimental results. They assumed that the dielectric constant of the medium around the particles is equal to that of the solvent ($\varepsilon_{m,water}$ = 1.77). In this paper, we will use the original shape factors of Gans theory, but with the dielectric constant of the medium, ε_m, as a variable. Studies by Miranda and Ahmadi (Miranda & Ahmadi 2005) and Gulati et al. (Gulati et al. 2006) indicate that the local dielectric properties have a strong influence on the optical absorption characteristics. The presence of a surfactant around the nanowires is one of the reasons why the dielectric constant can locally be different.

We believe that the chief advantage of Gans theory is the speediness of the calculations afforded by the simplicity of its formulation. The main alternative to the Gans approximation of other particle geometries makes use of the DDA method (Prescott et al. 2006; Brioude et al. 2005; Yin et al. 2006), which allows for different particle geometries but requires a significantly more difficult implementation with long computation times. Adapting Gans theory to real nanowires and nanoparticles samples would therefore have benefits in their characterization (Amendola V. & Meneghetti M. 2009).

In 2006, Eustis and El-Sayed already fitted calculated absorption curves to measurements in order to determine the aspect-ratio distributions for polydispersed samples (Eustis et al. 2006). By analyzing high-aspect-ratio nanowires, they could limit their analysis to the longitudinal plasmon resonance absorption. In this Chapter, we extend their work to determine the aspect-ratio distributions of gold nanowire solutions from measured absorption spectra for much-lower-aspect-ratio nanowires by taking the whole UV-vis absorption spectrum into account. Our results are compared with transmission electron microscope (TEM) images to confirm their validity, and we discuss the influence of the local environment of the nanowires. We will present suitable values for the effective dielectric constant of the medium based on our calculations using Gans theory. Finally, we will show that our method is also applicable to higher-aspect-ratio nanowires through a comparison with findings in the literature.

2. Calculation methods

The absorption coefficient, κ, for elongated particles was derived by Gans (Gans 1912) and implemented by Link et al. (Link et al. 1999) as in eq 1. The results in the initial publications of Link et al. contained a calculation error that was first noticed by Yan (Yan et al. 2003) and later corrected by Link and El-Sayed (Link & El-Sayed 2005).

$$k = \frac{2\pi NV\varepsilon_m}{3\lambda}\sum_{j=A}^{C}\frac{\left(1/P_j^2\right)\varepsilon_2}{\left(\varepsilon_1+\frac{1-P_j}{P_j}\varepsilon_m\right)^2+\varepsilon_2^2} \tag{1}$$

where N is the number of particles per unit volume, V is the average volume per particle, ε_m is the dielectric constant of the medium, λ is the absorbed wavelength, and $\varepsilon = \varepsilon_1 + i\varepsilon_2$ is the complex dielectric function of the prolate spheroid. The dielectric constant of the medium is related to the refractive index n by $\varepsilon_m \approx n^2$. For water ($n$ = 1.33), this gives ε_m = 1.77. The product NV equals the total volume of all particles. In eq 1, the depolarization or shape factors P_j relate the plasmon excitation to the aspect ratio of the particle for the three axes $j = A, B, C$ with lengths L_A, L_B, and L_C. For a prolate spheroid, this gives $L_A > L_B = L_C$. The usual notation for these shape factors (Gans 1912) as a function of aspect ratio $R = L_A/L_B$ is given by

$$\begin{aligned} P_A &= \frac{1-e^2}{e^2}\left(\frac{1}{2e}\ln\left(\frac{1+e}{1-e}\right)-1\right) \\ P_B &= P_C = \frac{1-P_A}{2} \\ e &= \sqrt{1-\frac{1}{R^2}} \end{aligned} \tag{2}$$

We use this formulation of the absorption of a prolate spheroid to approximate the absorption characteristics of gold nanowires.

Because of anisotropy, the nanowire absorption curves calculated with eqs 1 and 2 show two peaks associated with the longitudinal and transversal plasmon excitations. The position of the longitudinal absorption peak is strongly dependent on the aspect ratio of the particles as well as on the dielectric constant of the medium, ε_m.

Due to anisotropy, the absorption curves of nanorods show two peaks associated with the longitudinal (SP_{long}) and transversal (SP_{trans}) plasmon excitations. The position of the longitudinal absorption peak is strongly dependent on the aspect ratio of the particles as well as on the dielectric constant of the medium ε_m. Figures 1 and 2 show a redshift of the longitudinal absorption peak as the aspect ratio and ε_m increase. The transversal plasmon mode is also dependent on R and ε_m but the effect is much less pronounced. There is a slight blueshift when the aspect ratio increases and a redshift for higher values of the dielectric constant.

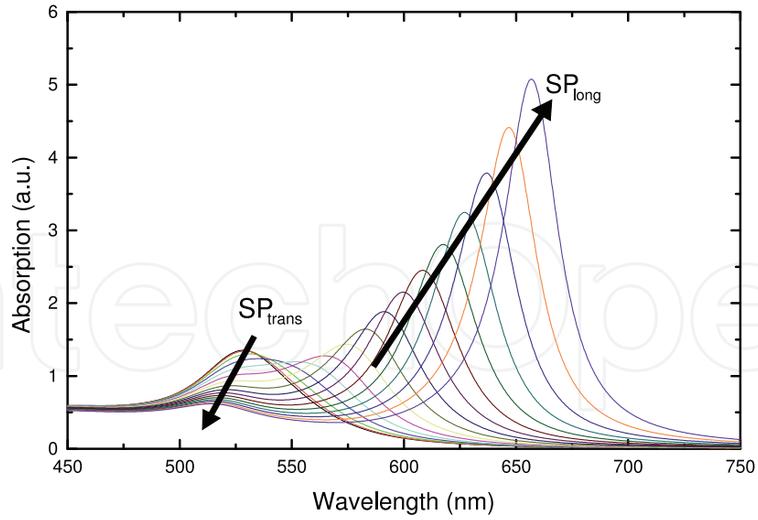

Fig. 1. Calculated absorption spectra for different aspect ratios $1 \leq R \leq 2.5$ with $\varepsilon_m = 2.1$. As the aspect ratio R increases, the transversal plasmon excitation SP_{trans} shows a slight blueshift and the longitudinal plasmon excitation SP_{long} shows a much stronger redshift.

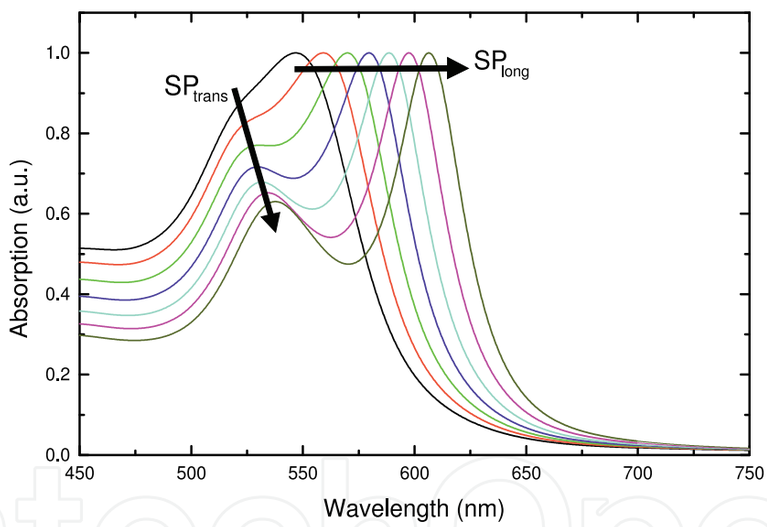

Fig. 2. Calculated absorption spectra for different dielectric constants $1.6 \leq \_m \leq 3$ with $R = 1.5$. There is a redshift for both SP_{trans} and SP_{long} as ε_m increases.

Because of this dependence of the absorption peak positions on the aspect ratio of the particles, we will observe a broadening of the absorption peaks when we analyze a solution containing nanowires of unequal size. By fitting the measured absorption curve with the calculated absorption curves of rods with different aspect ratios, we should be able to derive the original aspect-ratio distribution using methods similar to those employed by Eustis and El-Sayed (Eustis & El-Sayed 2006).

For a nanowire with aspect ratio R, the absorption as a function of the wavelength can be calculated using the formulation of Gans theory in eqs 1 and 2. Through the shape factors P_j, the absorption becomes dependent on the aspect ratio. Furthermore, we use the

dielectric constant of the medium, ε_m, as a fitting parameter; although the factor before the summation in eq 1 is merely a constant scaling factor, the value of ε_m within the summation has a profound effect on the shape of the absorption spectrum.

We used the complex dielectric constants $\varepsilon = \varepsilon_1 + i\varepsilon_2$ for bulk gold as obtained by Johnson and Christy (Johnson & Christy 1972). Recent studies (Stoller et al. 2006) have shown that there is a discrepancy between the dielectric constants of bulk gold and that of small gold particles. However, because the difference is small and the accuracy of the new results is limited, it is deemed sufficiently accurate to use the optical constants for bulk gold. The absorption curves are calculated for a series of aspect ratios and stored in a matrix *M*. This reduces our problem to solving $s = Mx$ for the aspect-ratio frequencies x, with vector s being our measured absorption spectrum. For real problems, there will not be an exact solution and we have to optimize the problem for a certain norm. Given the physical constraints of positive frequencies and smoothness of the solution, finding the solution becomes nontrivial. To optimize for a least-square error, we made use of a custom optimization algorithm implemented in the SCILAB 4.1 (INRIA & ENPC. Scilab 4.1 2006) software package. The calculated aspect ratio distributions are compared with size measurements from TEM images in order to confirm the validity of our calculation method.

Because we fit both the longitudinal and transversal plasmon excitation absorption peaks, we can analyze the size distributions of much-lower-aspect-ratio nanowires than previously reported. In the paper by Eustis and El-Sayed (Eustis & El-Sayed 2006), the fitting was limited to the longitudinal plasmon mode. The authors argued that the transversal absorption peak position is only weakly dependent on the aspect ratio of the particles and could therefore be ignored. In our studies, we used particles with aspect ratios $R \leq 2.5$, whereas Eustis and El-Sayed observed nanowires with $1.5 \leq R \leq 9$. This has two important consequences. When using much-lower aspect ratios, the importance of the blueshift of the transversal absorption peak increases as the redshift of the longitudinal absorption peaks diminishes. More importantly, there will be a larger overlap between the longitudinal and transversal absorption peaks. The intensity and position of the transversal absorption peak will then have an effect on the longitudinal absorption peak, and we cannot limit our analysis to only the longitudinal plasmon excitations. Instead, we must fit both peaks in the absorption curve at once. This requirement puts additional demands on the accuracy of the theory.

Fitting both absorption peaks also allows us to determine the abundance of spherical particles. However, a smaller range of aspect ratios will require a higher resolution and greater accuracy of the fitting algorithm in order to obtain a good fit to the experimental results. As such, by fitting both the longitudinal and transversal plasmon excitation absorption peaks, we should be able to accurately determine the full aspect-ratio distribution in our samples as well as the dielectric constant of the medium.

3. Experimental methods

3.1 Materials

Hydrogen tetrachloroaurate ($HAuCl_4 \cdot 3H_2O$, 99.5%) was purchased from Merck Co. Cetyltrimethylammonium bromide (CTAB, 99+%) was obtained from Acros Organics. Silver nitrate and ascorbic acid were from Wako Chemical Co. and Tokyo Kasei Co., respectively, and were used as received. Deionized water was used throughout the experiments.

3.2 Synthesis of gold nanowires

Gold nanowires were prepared by a seed-mediated growth method (Gou & Murphy 2005). More precisely, 9.5 mL of 0.1 M CTAB was combined with 0.5 mL of 0.01 M $HAuCl_4 \cdot 3H_2O$ and 55 μL of 0.1 M ascorbic acid as well as varying amounts (20, 60, and 100 μL) of 0.01 M silver nitrate aqueous solution, under continuous stirring. A seed solution was prepared according to Nikoobakht & El-Sayed 2003, and 12 μL of this solution was injected into the mixture to initiate the growth of gold nanowires. We obtained three different samples containing gold nanowires with different aspect-ratio distributions for the silver nitrate amounts of 20, 60, and 100 μL (samples 1-3). These samples were aged for 24 h in air to ensure full formation of gold nanowires.

3.3 Instruments

The absorption spectra of the nanowire solutions were measured with a Hitachi U-3500 spectrophotometer in the 300 to 900 nm range. TEM images were made with a JEOL JEM-2100F at 200 keV after a drop of the solution had been dried on a microarray.

4. Results

4.1 Experiments

The absorption spectra, measured for three different samples with different aspect-ratio distributions, are shown in figure 3. For sample 1, the longitudinal and transversal absorption peaks overlap to form one broad absorption peak. Two distinct peaks can be seen for samples 2 and 3, corresponding to the transversal plasmon mode at 520 nm and the longitudinal plasmon excitation around 600 nm.

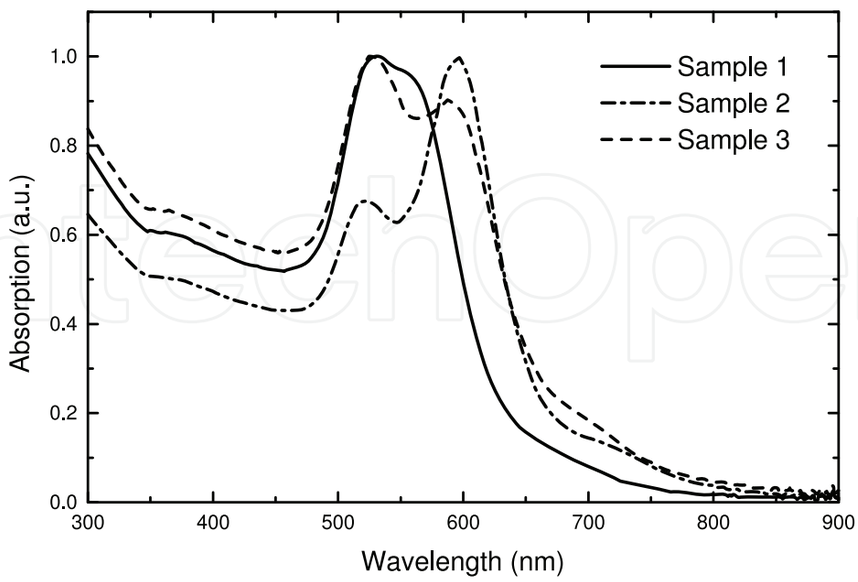

Fig. 3. Measured absorption spectra for three different aspect-ratio distributions. There is significant overlap between the longitudinal and transversal absorption peaks because of the low aspect ratios of the nanowires.

To validate our calculation methods, we have measured the size of the gold nanowires from TEM images. This enables us to later compare the calculated aspect-ratio distributions with the actual aspect ratios. Figure 4 shows the aspect ratios as determined from TEM images for more than 250 particles per sample. The lengths, L_A, and widths, L_B, were measured as the maximal length and width of the particles. For the three samples, the average particle lengths were L_A = 42, 46, and 40 nm and the average widths were L_B = 27, 25, and 22 nm. The standard deviation per sample was 15% for the widths and 12% for the lengths. The aspect ratio, R, is defined as $R = L_A/L_B$ as in the inset of figure 4. The peak aspect ratios for the rod-shaped particles were R = 1.5, 1.8, and 1.9 for samples 1, 2, and 3, respectively. The second peak in the distributions in figure 4 at $R \approx 1$ indicates the presence of spherical particles.

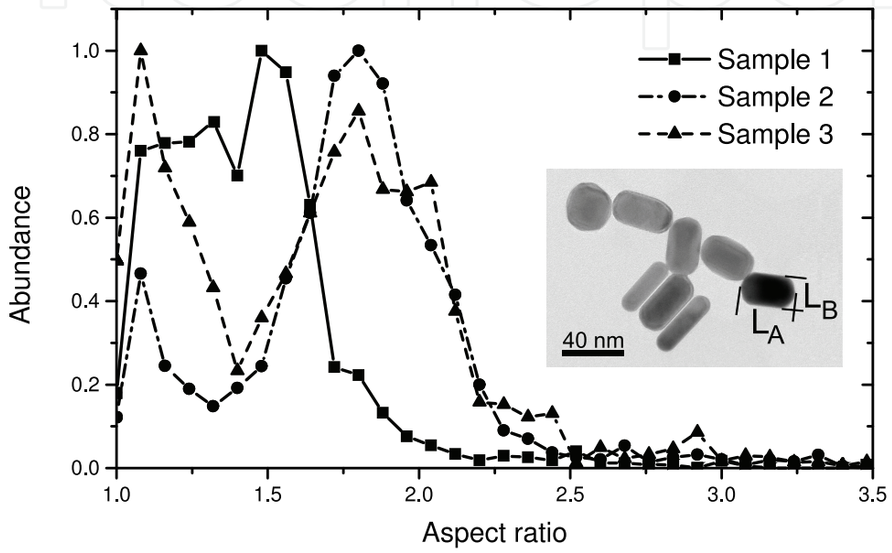

Fig. 4. Size distributions from TEM images. Curves are histograms of 253, 271, and 269 particles for samples 1, 2, and 3, respectively. The inset shows a characteristic TEM image (sample 3). The aspect ratio is given by $R = L_A/L_B$. High-aspect-ratio particles have a much smaller volume than low-aspect-ratio ones. Although the length, L_A, is constant, the width, L_B, is smaller for particles with a higher aspect ratio. An $R \approx 1$ particle can be seen on the top left.

It should be noted that the abundance in figure 4 was measured by particle volume because it is the volume of particles and not their count that defines the amount of absorption. We approximated the particle shape by using a spheroidally capped cylinder with an end-cap length of half the radius. However, the size distributions are such that the precise shape of the end caps has little influence on the total particle volume per aspect ratio. What is important is that the high-aspect-ratio particles ($R \geq 3$) are much smaller than particles with lower aspect ratios. As we can see in the inset of figure 4, particles with higher aspect ratios have lengths similar to the lower-aspect-ratio particles, but they are not as wide. The result is that the high aspect- ratio rods have a significantly smaller volume than the low-aspect-ratio ones and thus a smaller influence on the absorption spectrum. By taking the volume of the particles into account, we avoid overestimating the presence of the high aspect- ratio particles. The small shoulders at 700 nm in figure 3 should be attributed to these high-aspect-ratio particles ($R \geq 3$). Because eq 1 is not scaled by the number of particles, N, but rather by the total volume, NV, of the gold particles of a specific aspect ratio, R, we can transform our problem from determining the count of particles with a certain aspect ratio to determining the total volume

of all particles with a specific aspect ratio. Whenever we speak of abundance in this paper, we refer to the total volume of gold for all of the particles with a certain aspect ratio.

4.2 Calculations

For 100 aspect ratios between 1 and 4, we calculated the associated absorption curves using eqs 1 and 2. The measured absorption spectra of figure 3 were then fitted by a linear combination of these 100 different absorption spectra as can be seen in figure 5. For a series of ε_m, ranging from 1.7 to 2.4, the optimal fit to the absorption spectrum was determined and the fitting errors were plotted as a function of ε_m as in figure 6. The lowest fitting error then indicates the optimal dielectric constant. For samples 1-3, this gives us ε_m = 2.09, ε_m = 2.18, and ε_m = 2.12, respectively, which is significantly higher than the dielectric constant of the solvent $\varepsilon_{m,water}$ = 1.77. This dielectric constant corresponds to a refractive index of n = 1.46 ± 0.02. The quality of the fits is shown in figure 5, and it can be seen that the overall curve and the peak positions are fitted well, but there is a consistent deviation in the UV absorption. Additionally, the transversal absorption peaks are broader than Gans theory predicts. This appears to be a limitation of Gans theory. Our TEM images show the presence of several much larger, spherical particles. Because Gans theory does not include any size dependence of the absorption peak position and shape, the contribution of these particles to the absorption spectrum is ignored.

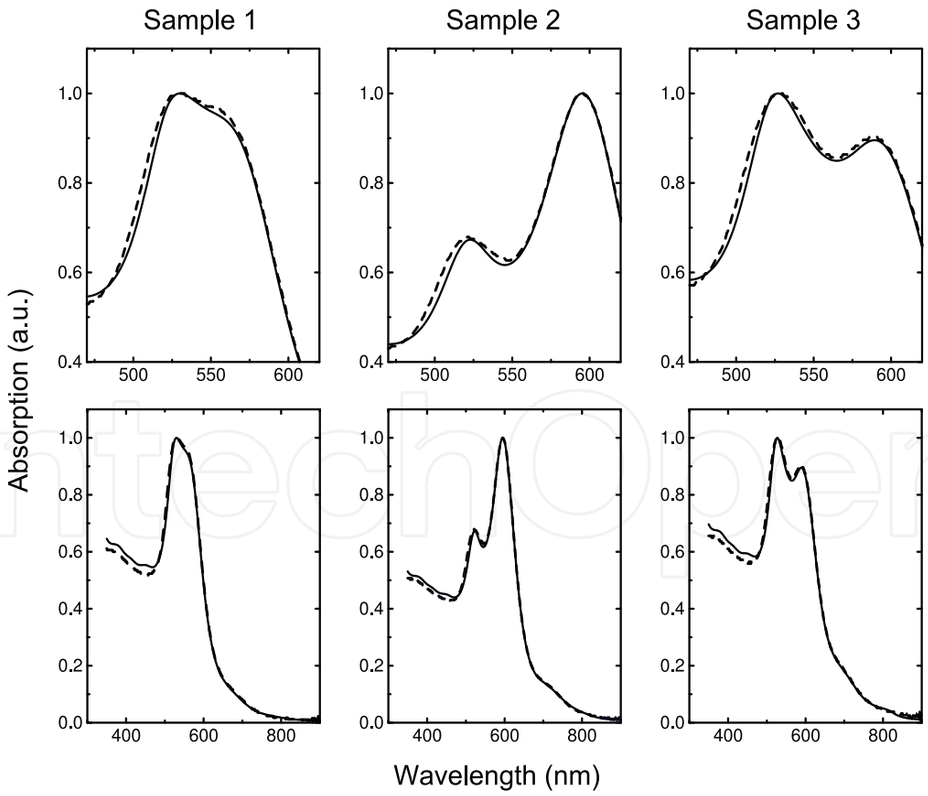

Fig. 5. Quality of Gans fitting with ε_m = 2.14 ± 0.05. Measured absorption spectra (dashed lines) and simulations (solid lines). The measured absorption spectra are a linear combination of the spectra of 100 particles with $1 \leq R \leq 4$.

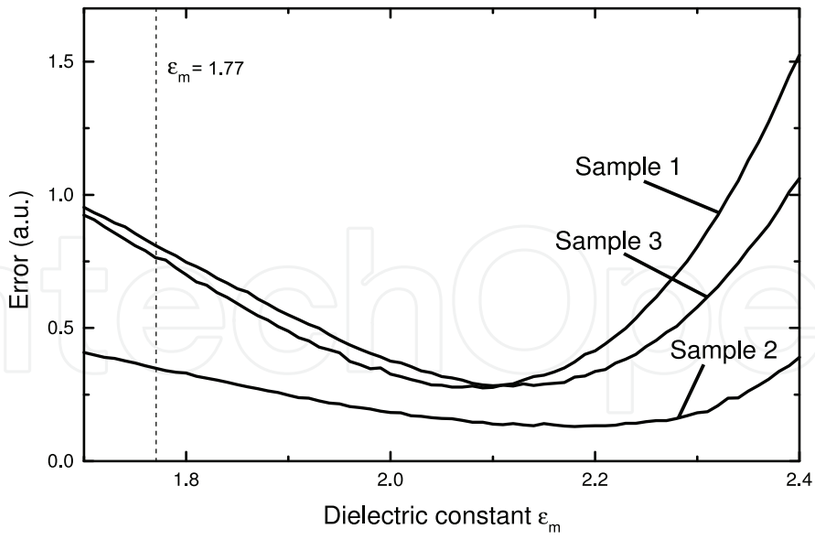

Fig. 6. Fitting errors per sample as a function of ε_m. The minimal fitting error indicates an optimal $\varepsilon_m \neq 1.77$. For the three samples, we find a minimal fitting error for $\varepsilon_m = 2.14 \pm 0.05$.

Figure 7 shows the results of the fitting using Gans theory, together with the aspect-ratio distributions as determined from TEM images. We can see that the peak aspect ratio for rodshaped particles ($R > 1.5$) matches our simulations for all three samples. Our fitting method thus gives a good approximation of the actual aspect-ratio distributions. It is clear that when we optimize the fitting of the absorption spectrum by adjusting ε_m we simultaneously optimize the fit to the measured aspect-ratio distributions. Apparently, our optimization of the medium dielectric constant in Gans theory is a necessary step in obtaining the correct aspect-ratio distributions.

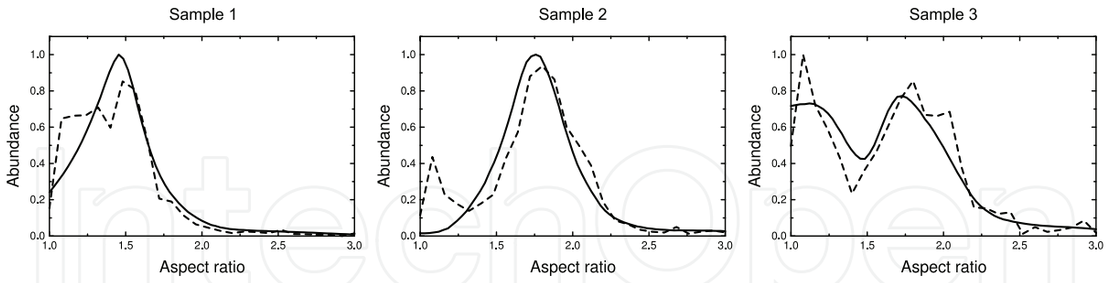

Fig. 7. Aspect-ratio distributions according to TEM images (dashed lines) and Gans theory (solid lines) for the optimized values of ε_m: $\varepsilon_m = 2.09$, $\varepsilon_m = 2.18$, and $\varepsilon_m = 2.12$ for sample 1, 2, and 3, respectively.

For samples 1 and 2, we see a deviation of the calculations from the TEM measurements for spherical particles ($R \approx 1$). The abundance of spherical particles in TEM images is larger for these samples than that suggested by our calculations. We can offer two possible explanations: either the applicability of Gans theory for spherical particles is limited or we overestimated the abundance of spherical particles in our TEM images. Nanowires that are standing perpendicular to the observation plane can be mistaken for spherical particles, possibly resulting in the disagreement for low aspect ratios for samples 1 and 2 in figure 7.

For sample 3, we do not observe such an effect. Here, the small disagreement between the TEM measurements and our fitting can be attributed to the limited number of particles measured. The simulation fits both aspect-ratio peaks at $R \approx 1$ and $R = 1.9$ to a good extent.

In the previous section, we did not need or use the TEM measurements to determine the aspect-ratio distribution or the dielectric constant of the medium. Nevertheless, to check the accuracy of the aforementioned value of ε_m and confirm the validity of our methods, we also calculated the absorption spectra with Gans theory given the particle size distributions as determined via TEM measurements. For every particle of which the aspect ratio and volume were determined from the TEM images, we calculate the absorption with eqs 1 and 2 and then sum these absorption spectra for all particles. This calculated absorption spectrum is compared with the measured absorption spectra in figure 3, while varying ε_m. Figure 8 shows the fitting results as well as the fitting errors as a function of ε_m. The optimal value of ε_m can again be determined by minimizing the fitting error. We find a good agreement between the calculated absorption spectra and the measured spectra from figure 3 for $\varepsilon_m = 2.1 \pm 0.1$. This matches the value of $\varepsilon_m = 2.14 \pm 0.05$ determined above by the inverse process.

It is possible to determine the aspect-ratio distribution of gold nanowires from an absorption spectrum using Gans theory if we optimize the dielectric constant of the medium. We can derive the optimal value of this dielectric constant from the absorption spectrum as well. Size measurements from TEM images confirm the accuracy of our method and support our hypothesis that the local environment of the particles has a significant influence on their optical characteristics.

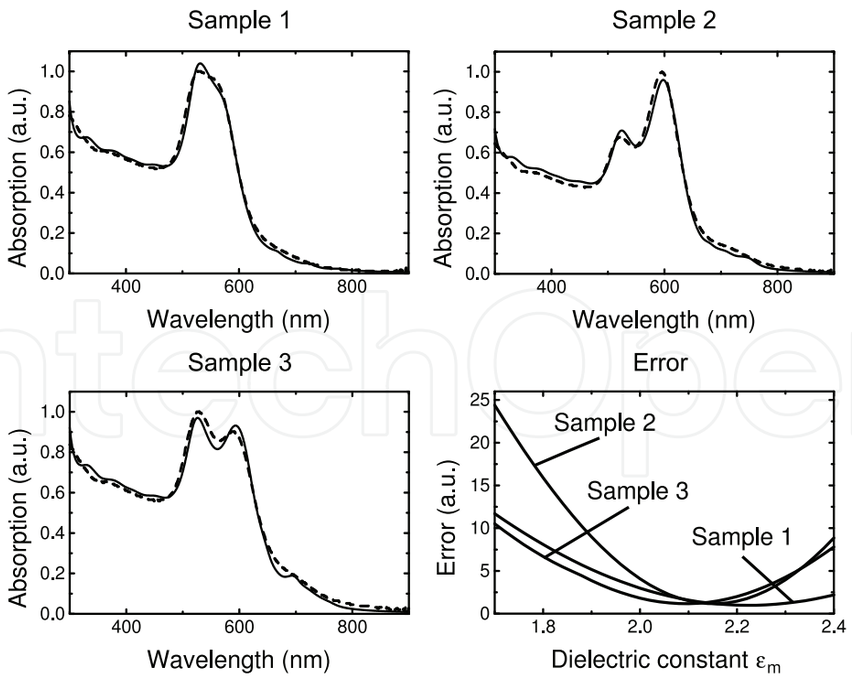

Fig. 8. Measured (dashed lines) and calculated (solid lines) absorption curves using the aspect ratios and volumes obtained from TEM images for the parameters R and NV in eqs 1 and 2. The fitting errors for the three samples are also given as a function of ε_m.

5. Comparison with other experimental results

5.1 Longitudinal peak position

Several studies use the longitudinal plasmon excitation absorption peak position to roughly determine the peak aspect ratio of nanowires in solution (Gulati et al. 2006; Zweifel & Wei 2005; Link et al. 1999; Yan et al. 2003; Link & El-Sayed 2005; Prescott & Mulvaney 2006; Brioude et al. 2005; Pérez-Juste et al. 2005). The wavelength of this absorption peak can be obtained with Gans theory by minimizing the denominator in eq 1 for the longitudinal shape factor P_A. Given that ε_2 is fairly constant in the UV-vis domain, the longitudinal absorption peak position is given by that wavelength, $\lambda_{\max}$, for which the following relation holds:

$$\varepsilon_1 = -\frac{1-P_A(R)}{P_A(R)}\varepsilon_m \tag{3}$$

Through linearization of eq 3, one can express the wavelength of the absorption maximum, $\lambda_{\max}$, of the longitudinal plasmon resonance as a function of the aspect ratio R and the dielectric constant ε_m. Using the method by Link et al. (Link et al. 1999), we found the following relationship for $\lambda_{\max}$:

$$\lambda_{\max} = (52.58R - 41.24)\varepsilon_m + 467.31 \text{ (nm)} \tag{4}$$

This is in good agreement with the results of Yan and co-workers (Yan et al. 2003).

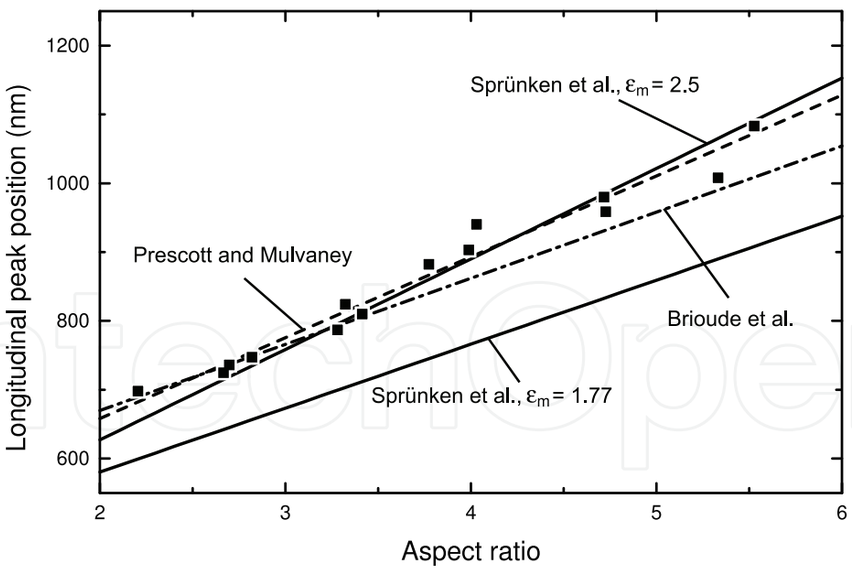

Fig. 9. Longitudinal peak positions as a function of nanowire aspect ratio. Experimental data from Pérez-Juste et al. (Pérez-Juste et al. 2005) (squares) compared with DDA calculations by Prescott and Mulvaney for a nanowire modeled as a cylinder (Figure 5 in Prescott & Mulvaney 2006) (dashed line), Brioude et al. (Figure 4 in Brioude et al. 2005) (dash-dotted line), and our simulations using Gans theory (solid line) with ε_m = 2.5 in eq 4. The solution of eq 4 for ε_m = 1.77 is given as a reference (bottom).

Figure 9 compares the experimental results of Pérez-Juste et al. (Pérez-Juste et al. 2005) with DDA calculations of Brioude et al. (Brioude et al. 2005) and Prescott and Mulvaney (Prescott & Mulvaney 2005), together with the predictions of Gans theory according to eq 4 for ε_m = 2.5. Equation 4 for ε_m = 1.77 is given as a reference. The DDA method has been used extensively in recent years to simulate gold nanowires. These studies used ε_m = 1.77 to calculate the longitudinal plasmon excitation peak positions. Figure 9 shows that, although there are some dissimilarities between the simulations of Brioude et al. and Prescott and Mulvaney, both calculations match the experimental results well. To obtain this good fit, Prescott and Mulvaney modeled the nanowires as cylinders, observing a significant dependence of the absorption characteristics on the particle geometry.

Using ε_m = 1.77, Brioude and co-workers reported (Figure 6 in Brioude et al. 2005)

$$\lambda_{\max} = 96R + 478 \text{ (nm)} \tag{5}$$

as a linear approximation of their simulation results. Equation 4 gives in this case $\lambda_{\max}$ = 93.07R + 394.3 (nm). The slope does not differ greatly, but there is a large offset of 80 nm. However, if we use ε_m = 2.5 instead of 1.77 in eq 4, we do find a good agreement between Gans theory and the experimental results of Pérez-Juste et al., as shown in figure 9. This requires a change of ε_m, but does not require changing the particle geometries. For the fittings of Brioude et al., Prescott and Mulvaney, and our simulation using Gans theory, we find sum square errors of 19×10^3, 5.7×10^3, and 9.9×10^3 (nm), respectively. Considering the experimental and calculation errors, all three fittings follow the experimental data well.

According to Prescott and Mulvaney (Prescott & Mulvaney 2006), the longitudinal surface plasmon mode is very sensitive to end-cap geometry. Their results, however, suggest that, even though the TEM images show the presence of spherical end caps (similar to our nanowires as in the inset of figure 4), one should model the nanowires as pure cylinders in order to obtain the best fit. Brioude et al. did not discuss the particle geometries used. We find that, by adjusting only the dielectric constant of the medium, we can also make Gans theory fit the experimental results of Pérez- Juste and co-workers without changing the nanowire geometries. We believe that this indicates that the dielectric constant of the medium plays as important a role as the particle geometry in the absorption characteristics of gold nanowires.

5.2 High-aspect-ratio nanowires

Eustis and El-Sayed (Eustis & El-Sayed 2006) also compared their TEM aspect-ratio measurements with Gans calculations, using ε_m = 1.77. They analyzed five samples with 1.5 ≤ R ≤ 9 and longitudinal absorption peaks at 630, 700, 850, 900, and 1000 nm (see figure 10). They only found a good match for two out of five samples, namely, for the samples with absorption peak positions of 630 and 900 nm (figure 5 in Eustis & El-Sayed 2006 and reproduced in figure 10). When one compares their measured absorption spectra with their measured aspect-ratio distributions, this is not surprising. Their two samples with longitudinal absorption peaks at 630 and 700 nm have very similar aspect-ratio distributions. The case for the samples with absorption peaks at 900 and 1000 nm is the same. When the measured

absorption spectra are dissimilar but the measured aspect-ratio distributions are similar, then the aspect-ratio distribution alone does not define the absorption spectra. This means that there must be another variable involved: either the local effective dielectric constant of the medium is different or the particle geometries are dissimilar.

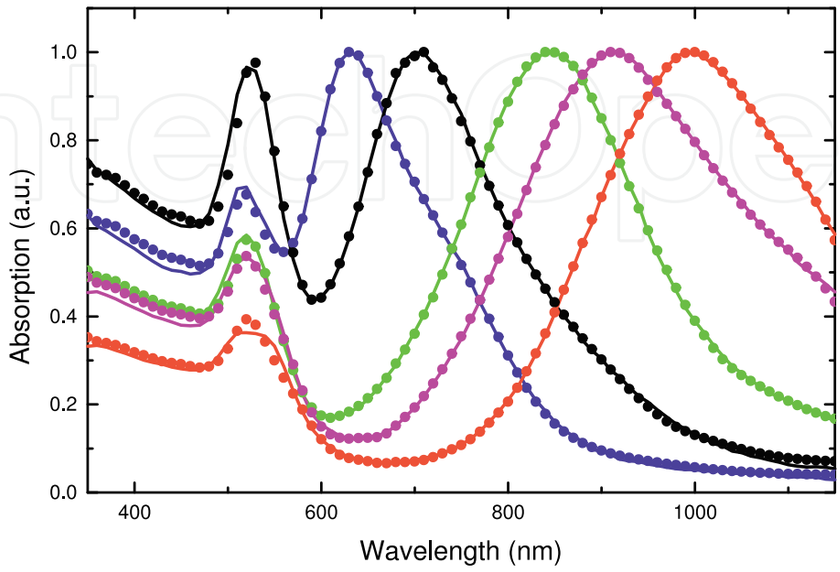

Fig. 10. Gans fitting (circles) using our method to absorption spectra (lines) by Eustis and El-Sayed from Fig. 5(c) in (Eustis & El-Sayed 2006).

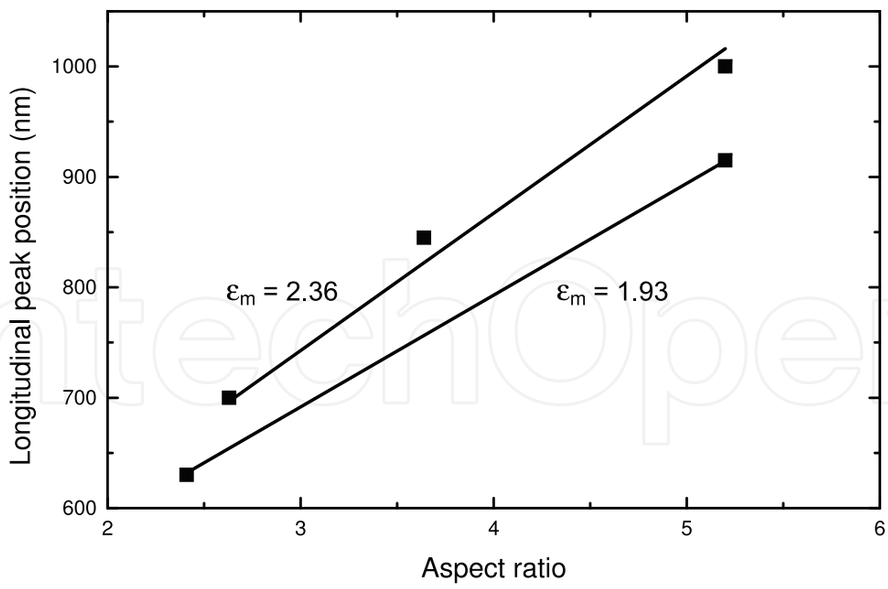

Fig. 11. Experimental data from Eustis and El-Sayed (Figure 5b in Eustis & El-Sayed 2006) (squares) fitted to eq 4 with $\varepsilon_m = 1.93$ (bottom) and $\varepsilon_m = 2.36$ (top).

Our results show that for $R \leq 2.5$ Gans theory allows for the determination of the aspect-ratio distribution of nanowires in solution, if we take the local dielectric environment of

the particles into account. Eustis and El-Sayed (Eustis & El-Sayed 2006) analyzed the size distributions of samples for a much-larger aspect-ratio range: $1.5 \leq R \leq 9$. To check the validity of Gans theory for higher aspect ratios, we also applied our fitting method with variable ε_m to their results. Using the dielectric constant of the medium as a fitting parameter, we found that we can fit all five absorption spectra if we define two values for ε_m. By fitting eq 4 to the longitudinal absorption peak positions of Eustis and El-Sayed as in figure 11, we find two sets of samples that are best modeled with two distinct values of ε_m.

For the samples with absorption peaks at 630 and 900 nm, we find $\varepsilon_m = 1.93$, whereas we find an optimal fit at $\varepsilon_m = 2.36$ for the samples with absorption peaks at 700, 850, and 1000 nm. This corresponds to the results of Eustis and El-Sayed, who found a reasonable fit for the first two samples, but did not find a good fit for the other three using $\varepsilon_m = 1.77$. In fitting eq 4 to the peak positions in figure 11, only the slope of the line can be varied by changing ε_m. between the experimental results and theoretical calculations. Through linearization of the longitudinal absorption peak position in Gans theory we obtain

$$\lambda_{max} = (52.58\mathrm{R} - 41.24)\varepsilon_m + 467.31 \text{ (nm)}. \tag{6}$$

All curves share a common point at $R = 0.78$ for which eq 4 reduces to $\lambda_{\max} = 467.31$ (nm). This means that, even for this limited dataset, we still have more data points than parameters in the curve fitting.

Figure 12 shows the aspect ratios as measured by Eustis and El-Sayed (Figure 5b in Eustis & El-Sayed 2006) compared to the fitting results for our method. Figure 12a shows the samples with absorption peaks at 630 and 900 nm, modeled with $\varepsilon_m = 1.93$. The samples with peaks at 700, 850, and 1000 nm, modeled with $\varepsilon_m = 2.36$, are shown in figure 12b. Note that these curves do not indicate the volume of particles but rather the count of particles. Eustis and El-Sayed (Eustis & El-Sayed 2006) reported that the volume of their nanowires was independent of the aspect ratio. From the good correspondence between the measured aspect ratios and our calculations in figure 12, it is reasonable to assume that we are dealing with two sets of samples that require different fitting parameters.

In other words, we can conclude that our fitting method is also applicable for high-aspect-ratio particles. Gans theory accurately describes the relation between the aspect-ratio distributions (Figure 12) and absorption spectra of Eustis and El-Sayed (Figure 5c in Eustis & El-Sayed 2006) without considering the particle geometries, when we regard ε_m as a fitting parameter.

The calculated aspect-ratio peak positions in Figure 12, as well as the shape of the curves, match the TEM measurements of Eustis and El-Sayed (Figure 5b in Eustis & El-Sayed 2006) well. It should be noted that for the sample with an absorption peak at 1000 nm (rightmost curve in figure 12b) there is a relatively large discrepancy between the experimental and theoretical results for $R > 5$. This is probably caused by the fact that for high aspect ratios and these values of ε_m the longitudinal absorption peaks fall outside of the spectral domain. The absorption spectra of Eustis and El-Sayed (Figure 5c in Eustis & El-Sayed 2006) are truncated at 1150 nm, which is lower than the longitudinal peak positions of the high-aspect-ratio

nanowires in our simulations. Another possible reason is that, as in our experiments, the nanowire volume might not be independent of aspect ratio, but smaller for high-aspect-ratio rods. As such, we may underestimate the count of high-aspect-ratio particles.

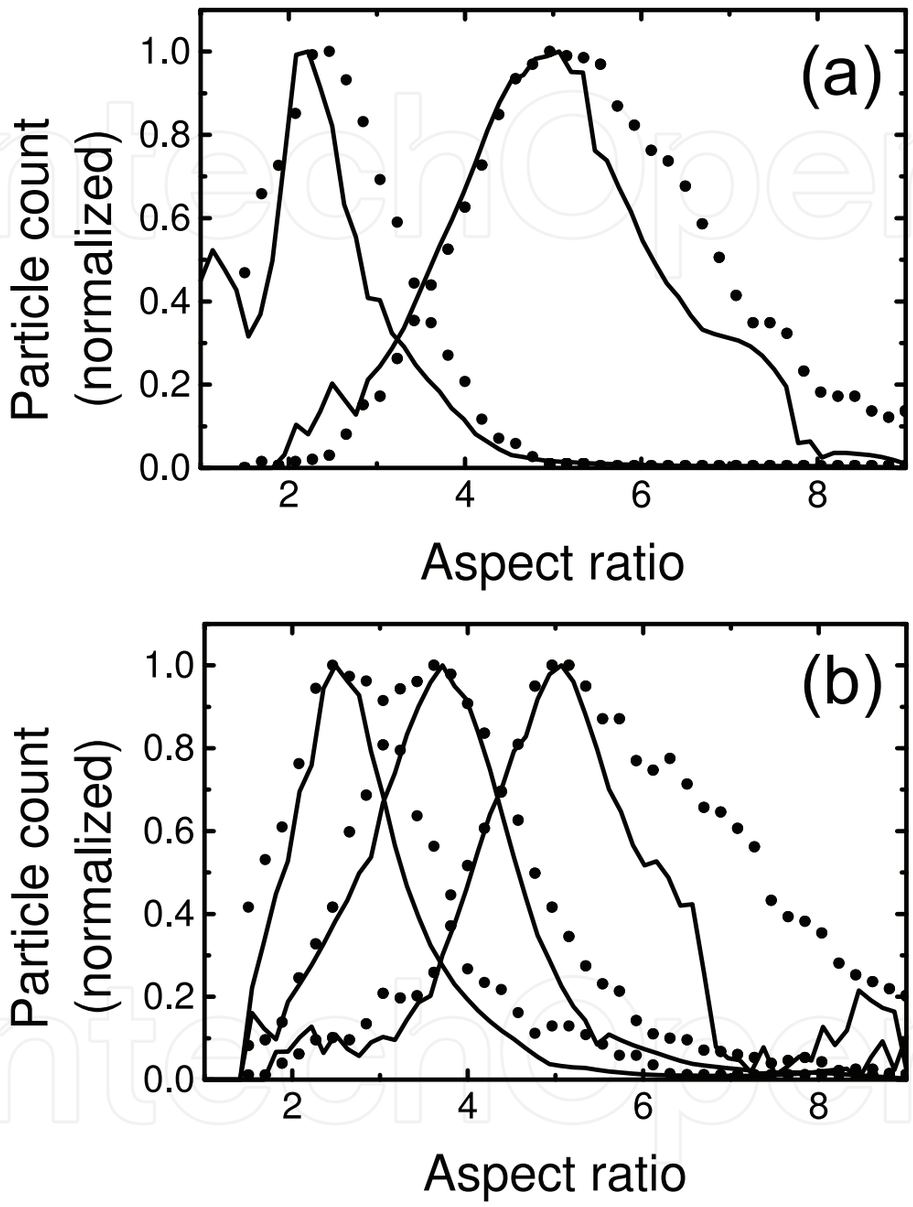

Fig. 12. Aspect-ratio distributions from TEM images by Eustis and El-Sayed (Figure 5b in Eustis & El-Sayed 2006) (squares) and from Gans fitting (solid lines) using our method with (a) $\varepsilon_m = 1.93$ and (b) $\varepsilon_m = 2.36$. The calculated absorption spectra using our fitting method are given in figure 10.

A comparison of our calculations with the absorption spectra of Eustis and El-Sayed (Figure 5c in Eustis & El-Sayed 2006) is given in figure 10. We find excellent agreement between our results and the measured absorption spectra.

6. Discussion

Using the dielectric constant of the medium as a fitting parameter, it is possible for one to obtain the aspect-ratio distribution of nanowires in solution from the absorption spectrum by fitting with Gans theory. To obtain a good match between the calculated aspect-ratio distributions and TEM measurements, we are required to set the dielectric constant of the medium to a significantly higher value than the dielectric constant of the pure solvent. For our gold nanowires with aspect ratios $R \leq 2.5$, we find that a value of $\varepsilon_m = 2.14 \pm 0.05$ gives a reasonable fit. However, the fitting has limited accuracy for very-low aspect ratios and thus it is hard to quantify the presence of spherical particles accurately. This could be the result of a limitation of Gans theory, but it can also be caused by errors in the size measurements from TEM images. We believe that the optical properties of the local nanowire environment are strongly affected by the presence of the surfactant as well as possible residue from the fabrication process. In analyzing the aspect ratios of nanowire-solutions, it has proven to be of great importance to incorporate a dependence on the dielectric properties of the local environment. We have shown that with Gans theory it is also possible to do this by optimizing the fit of the absorption spectrum for ε_m. In this way, one can not only determine the aspect-ratio distribution but also obtain insight into the local environment of the nanowires. Inversely, we have shown that Gans theory can be used to reproduce an absorption spectrum from a known particle size distribution. Here too, we find an optimal fit for $\varepsilon_m = 2.1 \pm 0.1$, which is significantly higher than the dielectric constant of water ($\varepsilon_m = 1.77$). This value for $\varepsilon_m = 2.1 \pm 0.1$ lies between the two values of $\varepsilon_m = 1.93$ and $\varepsilon_m = 2.36$ that we derived from the experimental results of Eustis and El-Sayed (Figure 5b and c in Eustis & El-Sayed 2006). The difference between the dielectric constants that we find for our particles and the experimental results of Pérez-Juste et al. could possibly be explained by differences in the nanowire synthesis procedures (see Pérez-Juste et al. 2005 and chapter 3).

We have analyzed particle sizes for a very small range of aspect ratios. Most contemporary research is done using particles with $R > 2$, whereas we have used particles with $R \leq 2.5$. The nanowires of Eustis and El-Sayed (Eustis & El-Sayed 2006) span a much larger range of aspect ratios ($1.5 \leq R \leq 9$), and when we apply our method to their results we also find a higher dielectric constant than expected for the solvent, as described in chapter 5. In fact, we need to define two different ε_m values in order to fit all of their experimental results. From their TEM measurements, it can be concluded that there is an additional variable besides the aspect ratio that influences the absorption spectrum. Three possible factors have been mentioned: end-cap geometry, particle size, and the dielectric constant of the medium. We have shown that Gans theory fits the results of Eustis and El-Sayed if we assume that not all samples have the same dielectric constant. A different dielectric constant could be the result of impurities in the solvent or different surfactant coverage densities of the nanowires. This could be the result of variations in the fabrication and growth process.

The results presented in this paper can probably be duplicated by using DDA calculations with varying particle geometries. We deem it likely that in reality a combination of these two effects occurs. In any case, the possibility that the dielectric constant of the medium in the vicinity of the nanowires is different from that of the pure solvent should not be easily

dismissed. It appears that adapting the particle geometry in DDA calculations does improve the agreement between theory and experiment but still does not fully explain the difference between Gans theory and experimental results (Prescott & Mulvaney 2006). A different dielectric environment around the nanowires could explain this discrepancy. Therefore, we believe that our results show that Gans theory is a useful tool in the determination of the aspect ratios of Au nanowires and offers a good alternative to the DDA method.

7. Conclusions

Our implementation of Gans theory provides a quick, easy, and nondestructive method to accurately obtain the aspect-ratio distributions of nanowire solutions from UV-vis absorption spectra. By optimizing the dielectric constant of the medium, ε_m, in our calculations, we obtain a good agreement with TEM measurements for low-aspect-ratio gold nanowires. We find that the dielectric constant of the medium is an important factor in the characterization of gold nanowires. A comparison of Gans theory with other experimental results also shows that a higher dielectric constant of the local environment of the nanowires improves the absorption spectrum calculations for a larger range of aspect ratios. The earlier work by Eustis and El-Sayed reported mixed results in applying Gans theory to inhomogeneously broadened absorption spectra (Eustis & El-Sayed 2006). We have improved on their methods and shown that their results can be explained better under the assumption that the dielectric properties of the local environment around the nanowires have a profound effect on the gold nanowire absorption characteristics (Sprünken et al. 2007).

8. Acknowledgment

We thank Mr. Daan Sprünken, Dr. Kazuaki Furukawa, Dr. Hiroshi Nakashima, Dr. Ilya Sychugov, Prof. Yoshihiro Kobayashi, Dr. Keiichi Torimitsu, Dr. Koji Sumitomo and Dr. Katsuhiro Ajito, Mr. Seiichiro Mizuno, Mrs. Hiroko Takahata for their comments, insightful discussions, and technical assistances. D.S. is supported through a Vulcanus in Japan scholarship by the EU-Japan Centre for Industrial Cooperation.

9. References

Agarwal, A.; Huang, S.-W.; Day, K.; O'Donnell, M.; Day, M.; Kotov, N. & Ashkenazi, S. (2007). Targeted Gold Nanorod Contrast Agent for Prostate Cancer Detection by Photoacoustic Imaging, *Journal of Applied Physics,* Vol. 102, No. 6, (September 2007), pp. 064701-1-3.

Amendola, V & Meneghetti (2009), Size Evaluation of Gold Nanoparticles by UV-vis Spectroscopy, *Journal of Physical Chemistry C* Vol. 113, No. 11, (February 2009), pp.4277-4285.

Brioude, A.; Jiang, X.; Pileni, M. (2005). Optical Properties of Gold Nanorods: DDA Simulations Supported by Experiments. *Journal of Physical Chemistry B* Vol. 109, No. 27, (June 2005), pp. 13138-13142.

Chen, C.-D.; Cheng, S.-F.; Chau, L.-K. & Wang, C. C. (2007). Sensing Capability of the Localized Surface Plasmon Resonance of Gold Nanorods. *Biosensers and Bioelectronics* Vol. 22, No. 6, (January 2007), pp. 926-932.

Eustis, S. & El-Sayed, M. A. (2006). Determination of the Aspect Ratio Statistical Distribution of Gold Nanorods in Solution from a Theoretical Fit of the Observed Inhomogeneously Broadened Longitudinal Plasmon Resonance Absorption Spectrum. *Journal of Applied Physics.* Vol. 100, No.4, (August 2006), pp. 044324-1-7.

Gans, R. (1912). Über die Form ultramikroskopischer Goldteilchen, *Annalen der Physik.* Vol. 342, No. 5, 881-900.

Gou, L. & Murphy, C. (2005). Fine-Tuning the Shape of Gold Nanorods, *Chemistry of Materials* Vol. 17, No. 14, (June 2005), pp. 3668-3672.

Gulati, A.; Liao, H. & Hafner J. (2006). Monitoring Gold Nanorod Synthesis by Localized Surface Plasmon Resonance, *Journal of Physical Chemistry B,* Vol. 110, No. 45, (October 2006), pp. 22323-22327.

Hu, M.; Wang, X.; Hartland, G.; Mulvaney, P.; Pérez-Juste, J. & Sader, J. (2003). Vibrational Response of Nanorods to Ultrafast Laser Induced Heating: Theoretical and Experimental Analysis, *Journal of American Chemical Society,* Vol. 125, No. 48, (November 2003), pp. 14925-14933.

INRIA & ENPC. *Scilab 4.1*, (2006) available from www.scilab.org.

Johnson, P. B. & Christy, R. W. (1972). Optical Constants of the Noble Metals, *Physical Review B*, Vol. 6, No. 12, (December 1972), pp. 4370-4379.

Link, S.; Mohamed, M. & El-Sayed, M. (1999). Simulation of the Optical Absorption Spectra of Gold Nanorods as a Function of Their Aspect Ratio and the Effect of the Medium Dielectric Constant, *Journal of Physical Chemistry B,* Vol. 103, No. 16, (April 1999), pp. 3073-3077.

Link, S. & El-Sayed, M. (2005). Simulation of the Optical Absorption Spectra of Gold Nanorods as a Function of Their Aspect Ratio and the Effect of the Medium Dielectric Constant, *Journal of Physical Chemistry B,* Vol. 109, No. 20, (May 2005), pp. 10531-10532.

Mie, G. (1908). Beiträge zur Optik trüber Medien, speziell kolloidaler Metallösungen, *Annalen der Physik,* Vol. 330, No. 3, pp. 377-445.

Miranda, O. & Ahmadi, T. (2005). Effects of Intensity and Energy of CW UV Light on the Growth of Gold Nanorods, *Journal of Physical Chemistry B*, Vol. 109, No. 33, (July 2005) pp. 15724-15734.

Murphy, C. J.; San, T. K.; Gole, A. M.; Orendorff, C. J.; Gao, J. X.; Gou, L.; Hunyadi, S. E. & Li, T. (2005). Anisotropic Metal Nanoparticles: Synthesis, Assembly, and Optical Applications, *Journal of Physical Chemistry B*, Vol. 109, No. 29, (June 2005), pp. 13857-13870.

Murphy, C. J.; Gole, A. M.; Hunyadi, S. E. & Orendorff, C. (2006). One-Dimensional Colloidal Gold and Silver Nanostructures, *Journal of Inorganic Chemistry,* Vol. 45, No. 19, (September 2006), pp. 7544-7554.

Nehl, C. L. & Hafner, J. H. (2008), Shape-dependent Plasmon Resonances of Gold Nanoparticles, *Journal of Materials Chemistry* Vol. 18, (February 2008), pp. 2415-2419.

Nikoobakht, B. & El-Sayed, M. (2003). Preparation and Growth Mechanism of Gold Nanorods (NRs) Using Seed-Mediated Growth Method, *Chemistry of Materials*, Vol. 15, No. 10, (April 2003), pp. 1957-1962.

Noguez, C. (2007). Surface Plasmons on Metal Nanoparticles: The Influence of Shape and Physical Environment, *Journal of Physical Chemistry C,* Vol. 111, No. 10, (February 2007), 3806-3809.

Orendorff, C.; Gearheart, L.; Jand, N. & Murphy, C. (2006). Aspect Ratio Dependence on Surface Enhanced Raman Scattering using Silver and Gold Nanorod Substrates, *Physical Chemistry Chemical Physics,* Vol. 8, No. 1, (October 2006), pp. 165-170.

Pérez-Juste, J.; Pastoriza-Santos, I.; Liz-Marzan, L. M. & Mulvaney, P. (2005). Gold Nanorods: Synthesis, Characterization and Applications, *Coordination Chemical Review*, Vol. 249, No. 17-18, (September 2005), pp. 1870-1901.

Prescott, S. W. & Mulvaney, P. (2006). Gold Nanorod Extinction Spectra, *Journal of Applied Physics,* Vol. 99, No. 12, (June 2006), pp. 123504-1-8.

Sönnichsen, C.; Franzl, T.; Wilk, T.; von Plessen, G.; Feldmann, J.; Wilson, O. & Mulvaney, P. (2002). Drastic Reduction of Plasmon Damping in Gold Nanorods, *Physical Review Letters* Vol. 88, No. 7, (January 2002), pp. 077402-1-4.

Stoller, P.; Jacobsen, V. & Sandoghdar, V. (2006). Measurement of the Complex Dielectric Constant of a Single Gold Nanoparticle, *Optics Letters,* Vol. 31, No. 16, (July 2006), pp. 2474-2476.

Sprünken, D; Omi, H; Furukawa K.; Nakashima H.; Sychugov I.; Kobayashi Y. & Torimistu K. (2007). Influence of the Local Environment on Determining Aspect-Ratio Distributions of Gold Nanorods in Solution Using Gans Theory, *Journal of Physical Chemistry C,* Vol. 111, No. 39, (September 2007), pp. 14299-14306.

Suzuki, M.; Niidome, Y.; Kuwahara, Y.; Terasaki, N.; Inoue, K. & Yamada, S. (2004). Surface-Enhanced Nonresonance Raman Scattering from Size- and Morphology- Controlled Gold Nanoparticle Films, *Journal Physical Chemistry B*, Vol. 108, No. 31, (July 2004), pp. 11660-11665.

Suzuki, M.; Niidome, Y.; Terasaki, N.; Inoue, K.; Kuwahara, Y. & Yamada, S. (2004). Surface-Enhanced Nonresonance Raman Scattering of Rhodamine 6G Molecules Adsorbed on Gold Nanorod Films, *Japanese Journal of Applied Physics,* Vol. 43, (April 2004), pp. 554-556.

Sztainbuch, I. W. (2006). The Effects of Au Aggregate Morphology on Surface-Enhanced Raman Scattering Enhancement, *Journal of Chemical Physics,* Vol. 125, No. 12, (September 2006), pp. 124707-1-12.

Xu, X.; Gibbons, T. & Cortie, M. (2003). Spectrally-selective Gold Nanorod Coatings for Window Glass, *Gold Bullutin*, Vol. 39, No. 4, pp. 156-165.

Yan, B.; Yang, Y. & Wang, Y. (2003). Comment on "Simulation of the Optical Absorption Spectra of Gold Nanorods as a Function of Their Aspect Ratio and the Effect of the Medium Dielectric Constant". *Journal of Physical Chemistry B*, Vol. 107, No. 34, (July, 2003), pp. 9159-9159.

Yin, G.; Wang, S.-Y.; Xu, M.; Chen, L. Y. (2006). Theoretical Calculation of the Optical Properties of Gold Nanoparticles, *Journal of the Korean Physical Society,* Vol. 49, No. 5, pp. 2108-2111.

Yu, C. & Irudayaraj, J. (2007). Multiplex Biosensor Using Gold Nanorods, *Journal of Analytical Chemistry,* Vol. 79, No. 2, (December 2007), pp. 572-579.

Zweifel, D. & Wei, A. (2005). Sulfide-Arrested Growth of Gold Nanorods, *Chemistry of Materials,* Vol. 17, No. 16, (June 2005), pp. 4256-4261.

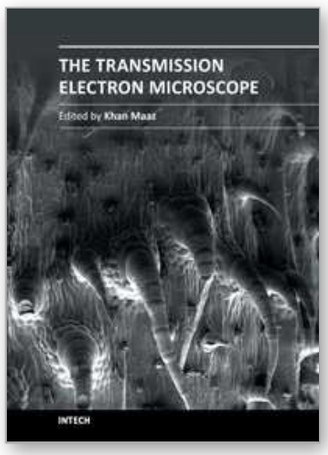

The Transmission Electron Microscope

Edited by Dr. Khan Maaz

ISBN 978-953-51-0450-6
Hard cover, 392 pages
Publisher InTech
Published online 04, April, 2012
Published in print edition April, 2012

The book "The Transmission Electron Microscope" contains a collection of research articles submitted by engineers and scientists to present an overview of different aspects of TEM from the basic mechanisms and diagnosis to the latest advancements in the field. The book presents descriptions of electron microscopy, models for improved sample sizing and handling, new methods of image projection, and experimental methodologies for nanomaterials studies. The selection of chapters focuses on transmission electron microscopy used in material characterization, with special emphasis on both the theoretical and experimental aspect of modern electron microscopy techniques. I believe that a broad range of readers, such as students, scientists and engineers will benefit from this book.

InTech Europe
University Campus STeP Ri
Slavka Krautzeka 83/A
51000 Rijeka, Croatia
Phone: +385 (51) 770 447
Fax: +385 (51) 686 166
www.intechopen.com

InTech China
Unit 405, Office Block, Hotel Equatorial Shanghai
No.65, Yan An Road (West), Shanghai, 200040, China
中国上海市延安西路65号上海国际贵都大饭店办公楼405单元
Phone: +86-21-62489820
Fax: +86-21-62489821

IntechOpen